Science of the Total Environment 810 (2022) 152210

Contents lists available at ScienceDirect

Science of the Total Environment

journal homepage: www.elsevier.com/locate/scitotenv

Nitrous oxide flux observed with tall-tower eddy covariance over a heterogeneous rice cultivation landscape

Yanhong Xie [a], Mi Zhang [a,b], Wei Xiao [a,b], Jiayu Zhao [a], Wenjing Huang [a], Zhen Zhang [a,d], Yongbo Hu [a], Zhihao Qin [a], Lei Jia [a], Yini Pu [a], Haoran Chu [a], Jiao Wang [a,e], Jie Shi [a], Shoudong Liu [a], Xuhui Lee [c,*]

[a] Yale-NUIST Center on Atmospheric Environment, International Joint Laboratory on Climate and Environment Change (ILCEC), Nanjing University of Information Science and Technology, Nanjing, Jiangsu Province, China

[b] Key Laboratory of Meteorological Disaster, Ministry of Education and Collaborative Innovation Center on Forecast and Evaluation of Meteorological Disasters, Nanjing University of Information Science and Technology, Nanjing, Jiangsu Province, China

[c] School of the Environment, Yale University, New Haven, CT, USA

[d] Nanjing Jiangning District Meteorological Bureau, Nanjing, Jiangsu Province, China

[e] Taiyuan Meteorological Bureau, Taiyuan, Shanxi Province, China

HIGHLIGHTS

- The rice-dominated landscape was a source of N_2O most of time.
- Temperature and precipitation were the main drivers of the N_2O flux variations.
- The N_2O flux was higher than those reported by other rice paddy studies.
- The emission factor was 3.8% in 2019 and 4.6% in 2020, respectively.

GRAPHICAL ABSTRACT

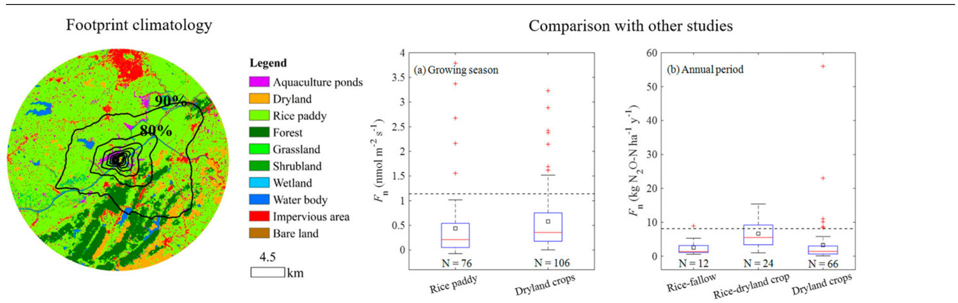

ARTICLE INFO

Article history:
Received 6 August 2021
Received in revised form 1 December 2021
Accepted 2 December 2021
Available online 8 December 2021

Editor: Anastasia Paschalidou

Keywords:
N_2O flux
Eddy covariance
Heterogeneous rice cultivation landscape
Emission factor

ABSTRACT

Although croplands are known to be strong sources of anthropogenic N_2O, large uncertainties still exist regarding their emission factors, that is, the proportion of N in fertilizer application that escapes to the atmosphere as N_2O. In this study, we report the results of an experiment on the N_2O flux in a landscape dominated by rice cultivation in the Yangtze River Delta, China. The observation was made with a closed-path eddy covariance system on a 70-m tall tower from October 2018 to December 2020 (27 months). Temperature and precipitation explained 78% of the seasonal and interannual variability in the observed N_2O flux. The growing season (May to October) mean flux (1.14 nmol m^{-2} s^{-1}) was much higher than the median flux found in the literature for rice paddies. The mean N_2O flux during the observational period was 0.90 ± 0.71 nmol m^{-2} s^{-1}, and the annual cumulative N_2O emission was 7.6 and 9.1 kg N_2O-N ha^{-1} during 2019 and 2020, respectively. The corresponding landscape emission factor was 3.8% and 4.6%, respectively, which were much higher than the IPCC default direct (0.3%) and indirect emission factors (0.75%) for rice paddies.

1. Introduction

With intensive application of nitrogen (N) fertilizer, agricultural lands are the largest anthropogenic source of atmospheric N_2O, accounting for more than 50% of the global anthropogenic N_2O emission (Tian et al., 2020). It is estimated that global N fertilizer use will increase by 50%

* Corresponding author.
E-mail address: xuhui.lee@yale.edu (X. Lee).

http://dx.doi.org/10.1016/j.scitotenv.2021.152210

from 2010 to 2050 in order to satisfy future food demand (Zhang et al., 2015). Increased N fertilizer utilization will promote soil microbial nitrification and denitrification processes and accelerate N_2O emissions. Based on a meta-analysis of 78 published studies, Shcherbak et al. (2014) find that N_2O emissions grow significantly faster than the linear relationship with N fertilizer application, with a typical emission factor (that is, the proportion of N in fertilizer application that escapes to the atmosphere as N_2O) of 0.99% ± 1.16% for dryland crops (mainly upland grain and N-fixing crops) and 0.28% ± 0.35% for rice paddies.

Field studies show that the N_2O flux in a cropland is dependent on agricultural management and environmental factors. Generally, the N_2O flux between the atmosphere and cropland soil increases with increasing soil moisture (Smith et al., 1998; Zheng et al., 2000) and shows linear or exponential relationships with temperature (Smith et al., 1998; Waldo et al., 2019). These functional relationships can be disrupted by large episodic emission events. In dryland crop systems, such as wheat, corn, cotton and canola, intensive N_2O fluxes are observed 1 to 20 days after N fertilizer application (Ding et al., 2007; Wagner-Riddle et al., 2007; Wang et al., 2013; Huang et al., 2014; Tallec et al., 2019; Waldo et al., 2019). High N_2O fluxes are also found after irrigation and heavy precipitation (Barton et al., 2011; Molodovskaya et al., 2012; Wang et al., 2013; Huang et al., 2014; Liang et al., 2018; Lognoul et al., 2019; Waldo et al., 2019). In rice paddies, larger flux is observed during short non-waterlogged periods than when the field is flooded (Akiyama et al., 2005; Zou et al., 2005; Qin et al., 2010; Yao et al., 2014). Continuous monitoring is essential to capture such emission episodes for accurate determination of the total N_2O emission from a cropland.

Flux chambers are a common method used to measure the N_2O flux in agricultural ecosystems. They are low-cost and relatively simple to operate, and can be replicated at multiple locations (Smith and Dobbie, 2001; Zheng et al., 2004). If automated and coupled to an in-situ N_2O gas analyzer, a chamber system can achieve a high degree of temporal and spatial coverage (Denmead et al., 2010; Barton et al., 2011; Butterbach-Bahl et al., 2013; Griffis et al., 2013; Tallec et al., 2019; Waldo et al., 2019). The majority of published chamber studies aim to measure the N_2O flux from cropland soils, which is the dominant pathway of direct emission. Indirect emissions occurring outside the target field, such as those associated with drainage networks, are generally missed by these measurements. In the UK agricultural land, drainage channels emit comparable amounts of N_2O as cropland soils, accounting for 86% of the total indirect N_2O flux (Outram and Hiscock, 2012). In the US Corn Belt, microstream channels emit 54 Gg N_2O-N y^{-1}, or 42% of the total agricultural N_2O emission in this region (Turner et al., 2015). A complete assessment of cropland N_2O budgets requires that the measurement system covers a footprint much larger than the typical plot scale (~1 m^2) for which flux chambers are suited.

An alternative method to flux chambers is eddy covariance (EC), which can provide long-term, continuous flux measurement. This approach has been used to investigate the N_2O flux in cropland (Christensen et al., 1996; Hargreaves et al., 1996; Skiba et al., 1996; Pattey et al., 2008; Molodovskaya et al., 2011; Molodovskaya et al., 2012; Wang et al., 2013; Huang et al., 2014; Rannik et al., 2015; Shurpali et al., 2016; Brown et al., 2018; Lognoul et al., 2019; Tallec et al., 2019; Cabral et al., 2020; Wang et al., 2020), grassland (Scanlon and Kiely, 2003; Di Marco et al., 2004; Leahy et al., 2004; Hsieh et al., 2005; Kroon et al., 2007; Neftel et al., 2007; Kim et al., 2010; Kroon et al., 2010a, 2010b; Mishurov and Kiely, 2011; Neftel et al., 2010; Jones et al., 2011; Hörtnagl and Wohlfahrt, 2014; Merbold et al., 2014; Wolf et al., 2015; Cowan et al., 2016; Fuchs et al., 2018; Liang et al., 2018; Cowan et al., 2020; Voglmeier et al., 2020; Goodrich et al., 2021), forests (Pihlatie et al., 2005; Eugster et al., 2007; Mammarella et al., 2010; Mishurov and Kiely, 2010; Pihlatie et al., 2010; Zona et al., 2013a, 2013b; Zenone et al., 2016) and urban ecosystems (Famulari et al., 2010; Järvi et al., 2014; Helfter et al., 2016). The in-situ or non-intrusive nature of the method is especially suited for capturing episodic emission events. For example, EC measurements observe significantly higher emission than chambers during a high-emission period in a cotton field due to irrigation (Wang et al., 2013). In the above cited studies, the EC system was deployed on short towers, measuring the flux from a footprint at the field or the ecosystem scale (~1 ha). Because the measurement tower was situated in a uniform field, the measured N_2O flux originated almost exclusively from direct emission of the target surface in question. Recently, Haszpra et al. (2018) documented the first results of N_2O flux monitoring with an EC system on a tall tower (measurement height 82 m), with a flux footprint of about 10 km in radius (Barcza et al., 2009). In the present study, an EC tower is considered to be tall if the flux footprint exceeds 10 km^2. Tall tower EC is desirable for a heterogenous agricultural landscape composed of multiple ecosystems and stream networks. Because of its large footprint, it allows observation of greenhouse gas fluxes integrated at the landscape scale (Davis et al., 2003; Haszpra et al., 2005; Desai et al., 2015; Peltola et al., 2015). In the case of N_2O, the tall-tower flux consists of emissions from agricultural soils as well as emissions in stream channels, thus providing a more complete assessment of the cropland N_2O cycle than flux chambers and short-tower eddy covariance.

In this paper, we present the results of the N_2O flux observation made with a closed-path EC system mounted on a tall tower in a cropland in the Yangtze River Delta (YRD), eastern China. YRD is one of the most intensive agricultural regions in China. Rice-winter wheat rotation is the major farming mode, which is supported by heavy N fertilizer use. Recent years have seen increasing aquacultural production, using aquaculture ponds converted from rice paddy fields. The landscape is highly heterogeneous. Mixed with rice/wheat fields are other surface features, including aquaculture ponds, vegetable fields, irrigation channels and water holding ponds. Generally, flooded rice paddy fields have lower N_2O flux than dryland crops. The emission factor for rice paddies is 0.68%, which is lower than 1.21% for wheat and 1.06% for maize according to 57 published studies (Linquist et al., 2012). This rice emission factor is based on chamber data; so far, no EC measurement has been attempted for rice paddies. Because irrigation channels are a prominent feature of rice cultivation, an open question is whether the emission factor at the landscape scale is greater than that for a single rice paddy.

To our best knowledge, the present study appears to be the first effort to measure N_2O flux with the EC method in a rice cultivation landscape (Nicolini et al., 2013; Nemitz et al., 2018). We aim (1) to assess the quality of flux data observed with the closed-path EC system on the tall tower, (2) to characterize temporal dynamics of the N_2O flux, (3) to investigate environmental factors that control the temporal variations of the N_2O flux, and (4) to obtain a N_2O emission factor for this rice paddy dominated landscape.

2. Materials and methods

2.1. Site description

The study site (118.2607 °E, 31.9672 °N, 11 m above sea level, Fig. 1c) is located in Quanjiao, Anhui Province, in the YRD. The region is under the influence of subtropical monsoon climate. The annual mean temperature and precipitation are 16.1 °C and 1091 mm (from 1990 to 2020), respectively. The prevailing wind direction at the site is between 45° and 135° (Fig. 1b). The landscape within a radius of 15 km is composed of cropland (rice paddy: 67.9%; dryland: 4.6%), forest (12.0%), aquaculture ponds (2.6%), water body (3.6%), impervious area (8.3%) and other land cover types (wetland, grassland, shrubland and bare land, 1.0%; Fig. 1a and Supplementary Table S1). Water body pixels include rivers, streams, water holding ponds and reservoirs. The Chuhe River, about 450 m from the site, flows through the flux footprint.

According to the governmental statistical yearbooks (http://tjj.chuzhou.gov.cn) and our field surveys, about 30% of the cropland in the flux footprint is double-cropped (Supplementary Table S2). Rice is usually transplanted in June and harvested in October, with a growing season of 120 to 130 days. Rice paddies are under conventional water management characterized by flooding in early season, mid-season drainage, and frequent waterlogging with intermittent irrigation in late season. Wheat is usually planted in November and harvested in next May. About 40% of

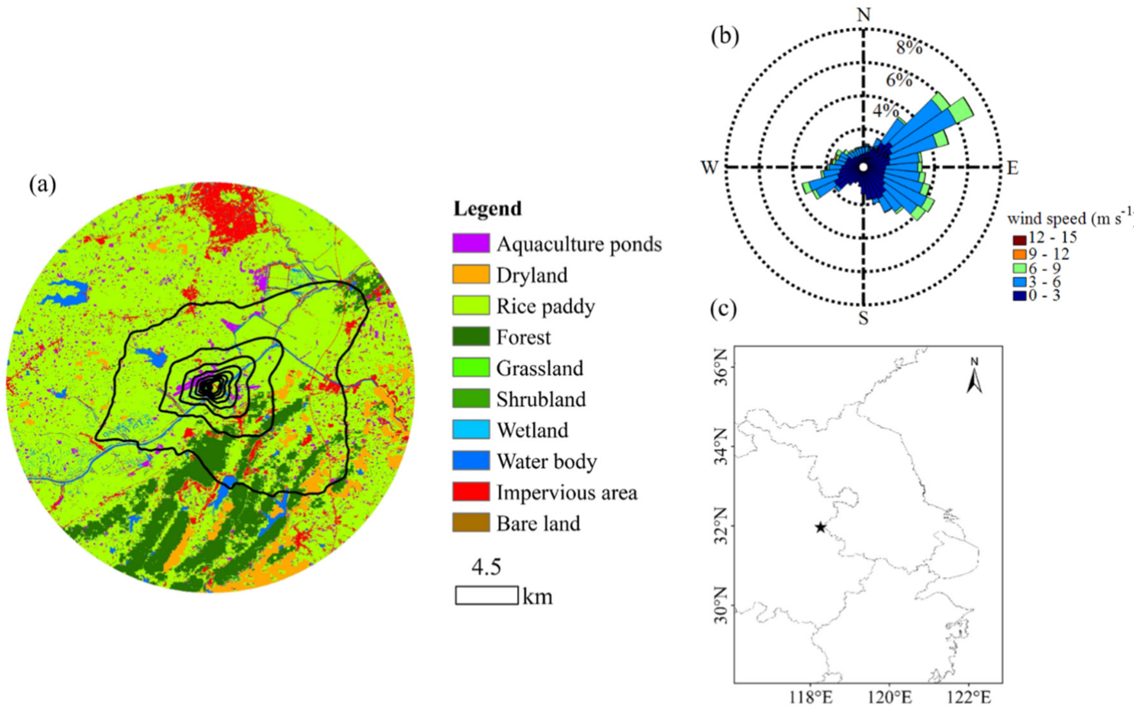

Fig. 1. Description of the field site. (a) Land use map (Gong et al., 2019) and footprint climatology over the whole measurement period. Contour lines represent footprint from 20% to 90% in a 10% interval. (b) Wind rose during the measurement period. (c) Map of the study site.

local farmers deploy rice-fallow rotation and 25% is shrimp farming in rice paddies. In rice-fallow rotation, rice is usually transplanted in middle May to early June and harvested in September. For shrimp farming, young shrimps are usually introduced into irrigation ditches near the rice paddies before rice harvesting. About 2 to 4 weeks after rice harvesting, the field is inundated to support shrimps which are usually harvested in next April to early June. Another 5% of the land is dryland crops, mainly vegetables.

Local farmers apply N fertilizers (compound fertilizer + urea) in May to middle June (for rice-fallow rotation) or June to middle July (for rice-wheat rotation and shrimp-rice farming) during the rice cultivation phase, at a rate of 110 kg N ha^{-1}. The N fertilizer use in wheat cultivation is applied in November and next February, with a total amount of 50 kg N ha^{-1}. The total annual N use is 160 kg N ha^{-1} in rice-wheat rotation. For shrimp-rice farming, soybean seed and commercial artificial diet are applied in March during shrimp cultivation phase, at amount of 2240 kg ha^{-1} (dry weight), corresponding to 130 kg N ha^{-1}. The total annual N use is 240 kg N ha^{-1} in shrimp-rice farming rotation. The amount of annual N use for vegetables is 160 kg N ha^{-1}. In aquaculture ponds, commercial artificial diet and chicken manure are used, with annual input of 18,000 kg ha^{-1} (dry weight) and 14,000 kg ha^{-1} (wet weight), respectively, equivalent to the total annual N input of 1430 kg N ha^{-1}, which is 5 to 12 times higher than in the cropland.

2.2. Instrumentation

Two EC systems were installed on a tower at the 70 m height above the ground (Fig. 2). One consisted of a closed-path CO_2/N_2O analyzer (model TGA200A, Campbell Scientific Inc., Logan, Utah, USA) and a three-dimensional ultrasonic anemometer (model CSAT3B, Campbell Scientific Inc.), and the other consisted of an open-path CO_2/H_2O analyzer (model EC150, Campbell Scientific Inc.) and a three-dimensional ultrasonic anemometer (model CSAT3A, Campbell Scientific Inc.). The closed-path EC system was installed in July 2018, and started to work normally in October 2018. The open-path EC system was in operation since June 2017. The EC signals were sampled at 10 Hz and stored by two dataloggers (models CR6 and CR3000, Campbell Scientific Inc.) for subsequent analysis. In parallel to the EC measurement, a trace gas analyzer (model G1301, Picarro Inc., Sunnyvale, CA, USA) was used to measure CH_4 and CO_2 concentrations from December 2017 to December 2018. The air inlet of this analyzer was placed at the same height of the EC systems. More details about the system for CH_4 and CO_2 concentration measurements are described by Huang et al. (2021).

The sampling setup of the closed-path EC system is shown in Fig. 2e. Its air inlet was located at the same height of the sonic anemometer at a distance of 8 cm from the center of the anemometer's path. The inlet was fitted with a vortex intake which served as a particulate filter: It divided the air into a dirty stream containing all the particles and a clean stream. Only the latter entered a dryer (Nafion® tube, 7.3 m long, 2.2 mm inner diameter, model TT-110, Perma Pure LLC, Lakewood, New Jersey, USA) and subsequently the analyzer's sampling cell. The dry air was drawn through a Teflon tube (75 m long, 6.35 mm inner diameter) at a nominal flow rate of 3.5 L min^{-1} at STP by a vacuum pump (model nXDS6i, Edwards Ltd., West Sussex, UK). The flow returning from the analyzer to the dryer and from the dryer to the pump occurred in a PVC suction hose (total length 140 m, 25.4 mm inner diameter). A needle valve between the dryer and the air sampling tube regulated the pressure of the whole system, which was kept at 35 to 39 mb. A reference gas of known concentrations (CO_2: 15,000 ppm, uncertainty: 1.5%; N_2O: 90 ppm, uncertainty: 3%) flew continuously through the reference cell of the analyzer, with a flow rate of 10 mL min^{-1}. On average, a 40 L reference cylinder lasted about 7 months. The light beam from the laser of the closed-path analyzer was split into its reference cell and the sample cell whose attenuation was measured by the same detector. The concentrations of the air sample in the sample cell were calibrated against the reference cell concentrations. The instrument uncertainties of the CO_2 and N_2O concentrations and fluxes were 1.5% and 3%, respectively.

In addition to the flux measurement, temperature and humidity were measured with temperature/humidity sensors (model HMP155, Vaisala Inc., Helsinki, Finland) at heights of 10, 50 and 70 m above the ground. Wind speed and wind direction were measured with anemometers and wind vanes (model 05103, R M Young Inc., Traverse City, Michigan, USA) at heights of 10 and 50 m. Air pressure was measured with a pressure sensor (model CS106, Campbell Scientific Inc.) at the height of 70 m. Four components of the surface radiation balance were measured with a radiometer (model CNR4, Kipp & Zonen B.V., Delft, the Netherlands) at the height

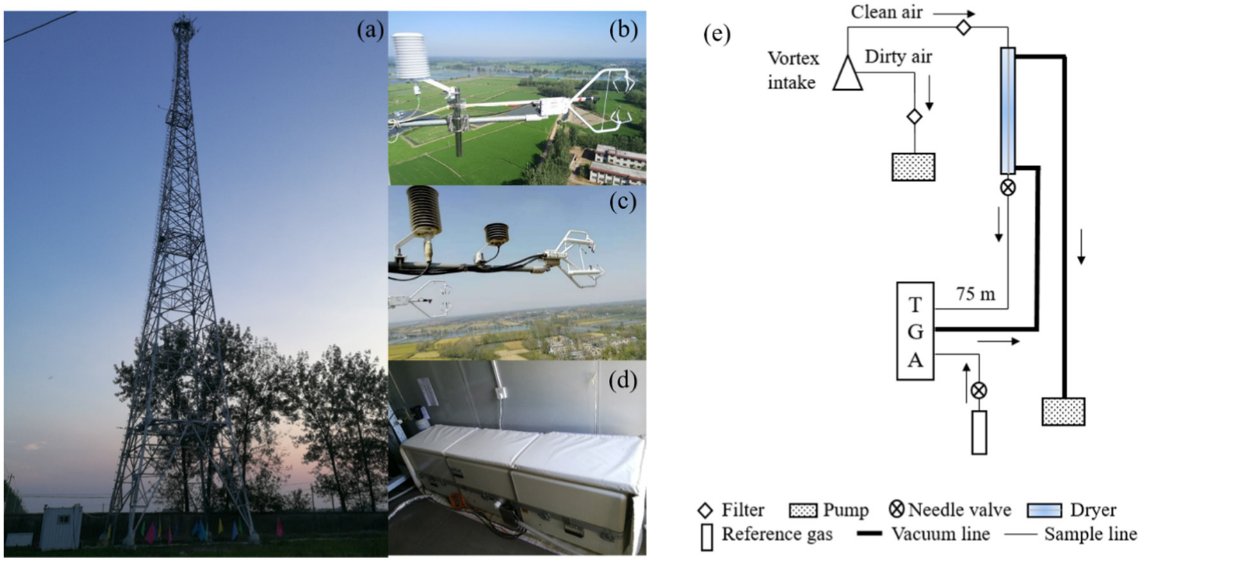

Fig. 2. Description of the EC systems. Photo of the flux tower (a), closed-path EC system: anemometer and the gas inlet (b), open-path EC system (c), N_2O/CO_2 gas analyzer (d), and schematic of sampling setup for the close-path EC system (e).

of 10 m. These meteorological variables were sampled by a datalogger (model CR3000, Campbell Scientific Inc.) and archived as half-hourly averages. Precipitation was monitored at a standard weather station maintained by the China Meteorological Data Network, located in Chuzhou City, about 30 km to the northeast of the study site. (The rain measurement at the tower was interrupted by large data gaps. For months with complete observation, the mean monthly precipitation at the tower was 65 mm, which is in good agreement with the mean value of 61 mm observed at the weather station for the same months.)

2.3. Data processing

Half-hourly fluxes were obtained with the EddyPro software (Version 6.2.1, LI-COR Inc., Lincoln, Nebraska, USA) from the 10 Hz EC data. Before the flux calculation, the raw data were screened for spikes (Vickers and Mahrt, 1997). A double coordinate rotation was used to remove tilt errors (Aubinet et al., 2012). The lag time caused by spatial separation of the gas analyzer and the sonic anemometer (and by travel through the sampling tube for the closed-path EC) was corrected before the flux calculation. The lag time was determined with a covariance maximization method supplemented with a default value and a preset range of allowable values (Aubinet et al., 2012; more on this in Section 3.1). The WPL density correction was applied to the open-path EC gas fluxes (Webb et al., 1980). No density correction was needed for the closed-path system as temperature fluctuations were removed by the sampling tube and water vapour was removed by the dryer. The Reynolds number of the flow in the sampling tube was about 2250, which is close to the critical Reynolds number of 2300, indicating some loss of high-frequency fluctuations. Hence, a spectral correction method was used to correct for the flux loss at high frequencies caused by dynamic frequency response of the sensor, scalar and vector path averaging, sensor separation and signal attenuation down the sampling tube (Moncrieff et al., 1997).

The eddy flux was corrected for the storage term below the measurement height using the concentration time series measured by the analyzer. This correction could be subject to errors at the sub-day time scale because it was not based on profile measurements, but the uncertainty was not as critical at longer time scales. The 0-1-2 quality flag system developed by Mauder and Foken (2004) was used to remove poor quality flux data (data tagged with flag 2). The nighttime fluxes were screened for conditions of possible decoupling between the surface and the air layer. Half-hourly observations whose friction velocity (u_*) was less than 0.1 m s^{-1} were excluded from further analysis. The threshold was determined by the relationship between the nighttime CO_2 flux and the friction velocity (Aubinet et al., 2012).

Our analysis focused on flux values at the daily, monthly and annual timescales. Processes at sub-day timescales, such as convective mixing during morning transitional periods (Peltola et al., 2015), were omitted from the results presented below. The closed-path EC was interrupted by occasional power failures and equipment maintenance. After data quality screening, valid N_2O flux data was obtained for 48% half-hourly intervals from October 2018 to December 2020. A daily mean flux was calculated if there was 50% or more valid half-hourly flux data in that day. The overall daily data coverage was 63%. Since there were three large data gaps (9 March to 29 April 2020, 52 days; 28 June to 12 August 2020, 46 days; 13 to 31 December 2020, 19 days), gaps were filled on monthly scale. A monthly mean N_2O flux was calculated if valid daily flux data exceeded 50% in that month. For other months, gaps were filled by a multiple nonlinear regression equation between the observed monthly N_2O flux and monthly mean air temperature and precipitation (Section 3.3). Annual cumulative N_2O emission was calculated from the gap-filled monthly data.

2.4. Footprint analysis

The EC flux footprint was calculated for every half hour using the footprint model of Kljun et al. (2015). The input parameters include the EC measurement height, roughness length, wind speed, boundary layer height, the Obukhov length, crosswind standard deviation, friction velocity, and wind direction. Surface roughness was estimated from the linear relationship between wind speed and friction velocity (Lee, 2018). Boundary layer height data was obtained from NOAA's global data assimilation system (https://ready.arl.noaa.gov/gdas1.php). All other input data were provided by the EC systems. The footprint climatology based on the hourly flux footprint (Fig. 1a), was used to upscale fertilizer application data for comparison with the N_2O flux. The upscaling was carried out at the annual timescale and for the whole flux footprint.

2.5. Plot- and field-scale data from published studies

We compared our tall-tower flux with plot- and field-scale data found in 81 published studies (Supplementary Tables S3 and S4). For comparison of the mean flux measured in the growing season, the data were divided into two groups: rice paddy versus dryland crops. Here dryland crops include grain crops (wheat, corn and soybean) and commercial crops (cotton, rapeseed, sugarcane and sugar beet). For comparison of the annual mean flux, the data were grouped into three categories (rice-fallow, rice-dryland crop rotation and dryland crops).

3. Results

3.1. Quality assessment of the closed-path EC data

The long sampling tube (75 m, Fig. 2e) used by the system caused a large lag time. Here the lag time was determined with the lagged correlation between the 10 Hz CO_2 signal and the vertical velocity for every half-hourly period. Fig. 3 shows the lagged correlation for several afternoon periods in August 2019. During these periods, the CO_2 flux signal was strong (from -7.58 to -40.16 μmol m^{-2} s^{-1}), representing ideal conditions for the lag time determination. The result indicated a highly stable time lag of 7.4 ± 0.1 s. Accordingly, the default lag time was set to 7.4 s in the EddyPro software. As the tube flow rate could vary with pressure, the lag time was allowed to fluctuate between 7.0 and 8.5 s. If the lag correlation calculation returned a lag time outside this range, the default value was used. Over the whole experimental period, above 70% of the half-hourly observations had a lag time in the 7.0 to 8.5 s window, indicating a stable flow rate through the analyzer.

We used the CO_2 time series for the determination of time lag because its signal was much stronger than the N_2O time series, resulting in a more precise estimate of the time lag. We then assumed the same lag time for N_2O. This is a safe assumption because N_2O is an inert gas without evidence of an adhesion tube-wall effect. The same method of lag determination can be found in Kroon et al. (2010a), Rannik et al. (2015) and Brown et al. (2018), who used CO_2 or CH_4 to estimate the lag time for N_2O.

The N_2O flux was weakly sensitive to the lag time. If the default lag time was used for all observational periods, the mean N_2O flux would decrease by 5%. The weak sensitivity was an indication that turbulent diffusion at the measurement height (70 m above the ground) was dominated by large eddies.

Typical co-spectra between the vertical velocity and three scalars (temperature, CO_2, and N_2O) are shown in Fig. 4. Overall, the co-spectra were in good agreement with the ideal co-spectral model proposed by Kaimal et al. (1972), especially for temperature and CO_2. The N_2O co-spectrum was noisier than those of temperature and CO_2, and appeared to be lower than the modelled value for normalized frequency greater than 3, emphasizing the need for high frequency correction. (The frequency correction by the EddyPro software increased the N_2O flux by 10% on average.)

Fig. 5a shows the half-hourly turbulent CO_2 flux time series observed with two EC systems for a typical 7-day period and Fig. 5b is a 1:1 comparison of these two systems for the whole measurement period. The CO_2 flux measured by the closed-path system agreed well with that from the open-path system (R^2 = 0.88; Fig. 5b). Further, in Fig. 6,

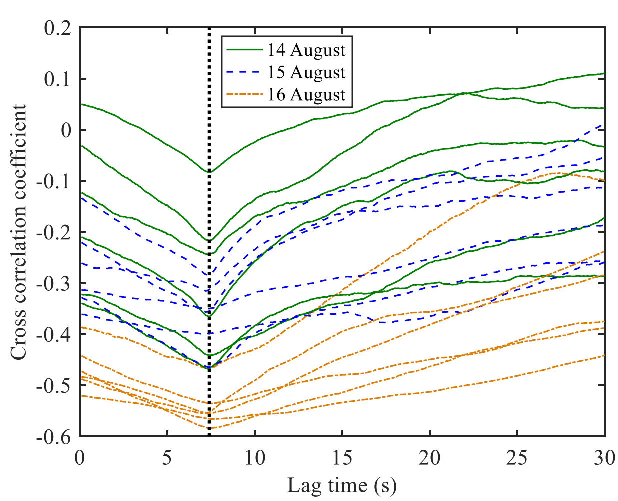

Fig. 3. Lagged correlation between the CO_2 concentration and the vertical velocity. Observations were made between 12:00 and 15:00 local time on 14 to 16 August 2019. The black dotted line represents a lag time for 7.4 s. Each data curve represents a half-hourly observation.

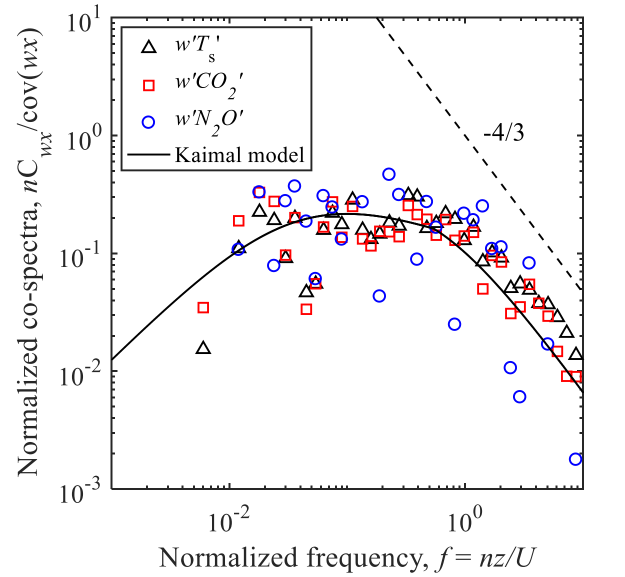

Fig. 4. Normalized co-spectra between the vertical velocity (w) and sonic temperature (T_s), CO_2 concentration and N_2O concentration for 12:00–15:00, 18 September 2019. The x axis is normalized frequency, where n is natural frequency, z is measurement height and U is wind speed. The black solid curve represents the ideal co-spectral model of Kaimal et al. (1972), and black dashed line represents the ideal slope of $-4/3$ in the inertial subrange.

CO_2 concentration observed by the closed-path analyzer is compared with that obtained with the Picarro system over a two-month period (14 October to 21 December 2018) when both were functioning normally. Once again, an excellent agreement was achieved, as evidenced by the good correlation (R^2 = 0.997) and a small difference of 1% between the two systems (Fig. 6b).

The CO_2 comparisons indicated that the closed-path EC system achieved a high standard of performance. Since the N_2O and CO_2 measurements were made with the same laser, detector and plumbing setup, a reasonable inference is that its N_2O flux data was also in good quality. Brown et al. (2018) reported that excellent agreement was achieved for both the CO_2 and the N_2O fluxes measured with a closed-path EC system of the same type as ours and with two other parallel EC systems.

3.2. Temporal variations of the N_2O flux

Time series of the daily and monthly N_2O flux are shown in Figs. 7 and 8, along with the daily and monthly air temperature and precipitation. The daily mean temperature varied from -4.3 to 34.7 °C over the measurement period. The annual mean air temperature was similar between the two years (18.2 °C in 2019 and 18.0 °C in 2020). More precipitation fell in the summer of 2020 than in 2019: the annual precipitation in 2020 was 1322 mm, which more than doubled the amount in 2019 (564 mm). Year 2019 was the second driest year in the period from 1990 to 2020, and year 2020 was slightly wetter than the climate norm (1091 mm). The largest daily precipitation was 98.2 mm (recorded on 8 August 2020). The summer total precipitation (830 mm, June to August) in 2020 was the third highest during the period from 1990 to 2020.

The daily N_2O flux was highly variable with time, ranging from -0.96 (on 8 February 2019) to 4.91 nmol m^{-2} s^{-1} (20 August 2020; Fig. 7a). The overall daily mean N_2O flux was 0.90 ± 0.71 nmol m^{-2} s^{-1} (mean ± 1 standard deviation). Negative daily flux occurred on 39 days, mostly in the winter and the spring.

The observed monthly mean flux varied from 0.34 nmol m^{-2} s^{-1} in January in 2019 to 1.84 nmol m^{-2} s^{-1} in June in 2020 (Fig. 8a). The flux in the summer (June to August) of 2020 (1.68 ± 1.07 nmol m^{-2} s^{-1}) was 49% higher than in the summer of 2019 (1.13 ± 0.62 nmol m^{-2} s^{-1}). This difference was most likely caused by precipitation variations: the total

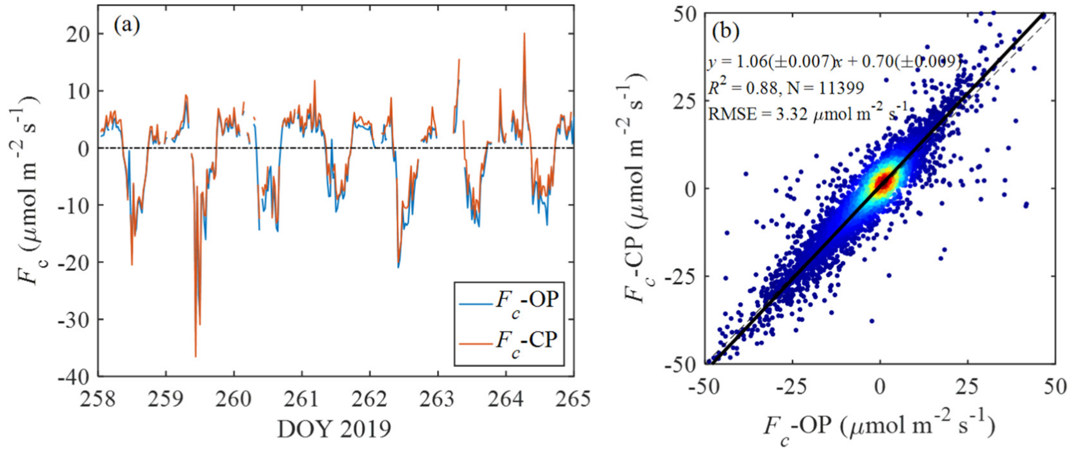

Fig. 5. Comparison of the CO_2 flux observed with two EC systems (OP: open-path, CP: closed-path). (a) Time series for a typical 7-day period, (b) 1:1 plot for the whole measurement period. In panel b, color indicates data density. Also shown in panel b are regression statistics.

precipitation in the summer of 2020 (830 mm) was more than 4 times that in the summer of 2019 (191 mm; Fig. 8b). The mean flux during the rice growing season (May to October) was 1.14 ± 0.72 nmol m^{-2} s^{-1}, which was about twice that observed in non-growing season (0.63 ± 0.59 nmol m^{-2} s^{-1}; November to April).

The half-hourly N_2O flux did not show obvious diurnal patterns (Fig. 9). For example, the difference between the mean daytime flux (1.07 ± 4.64 nmol m^{-2} s^{-1}; solar elevation angle > 0°) and the nighttime flux (1.02 ± 2.68 nmol m^{-2} s^{-1}; solar elevation angle < 0°) in the autumn was within their ranges of variations.

The annual cumulative N_2O emission was 7.6 kg N_2O-N ha^{-1} in 2019 and 9.1 kg N_2O-N ha^{-1} in 2020. The cumulative emission from the growing season (May to October) of 2019 and 2020 was 5.1 and 6.1 kg N_2O-N ha^{-1}, respectively, which contributed about 67% of the total annual emission. A Monte-Carlo simulation was used to estimate the uncertainty of the annual flux arising from gap-filling. This simulation was based on 10,000 ensemble members and the assumption that errors of the regression coefficients (Section 3.3) followed a normal distribution, and their standard deviations were all taken as 50% of the 95% confidence intervals. The standard deviation of the simulated annual N_2O flux was 0.20 nmol m^{-2} s^{-1}, which was equivalent to 22% of the mean observed N_2O flux over the whole measurement period.

3.3. Effects of environmental conditions on the N_2O flux

Fig. 10 shows the dependence of the N_2O flux on air temperature at the daily, 10-day and the monthly scale. The relationship with air temperature was exponential at these three time scales and the correlation was significant ($R^2 > 0.15$, $p < 0.01$). A notable outlier was found in the monthly flux versus temperature relationship (panel c); it occurred in June 2020, a month with very high precipitation (291 mm). A two-variable regression on the monthly data yields,

$$F_n = -1.397(\pm0.205)e^{-0.068(\pm0.051)T_a} + 0.003(\pm0.001)P + 1.204(\pm0.385) \quad (1)$$

where F_n is monthly flux in nmol m^{-2} s^{-1}, T_a is air temperature in °C, P is precipitation in mm, and the parameter bounds denote 95% confidence intervals. This regression explained 78% of the observed flux variability, better than the single variable regression with temperature ($R^2 = 0.63$, Fig. 10c).

3.4. Comparison with plot- and field-scale flux data

Fig. 11 shows a comparison of the flux value in this study with plot- and field-scale N_2O flux data for the growing-season and the annual period found in the literature. The growing season N_2O flux is 0.44 ± 0.70 (mean ±

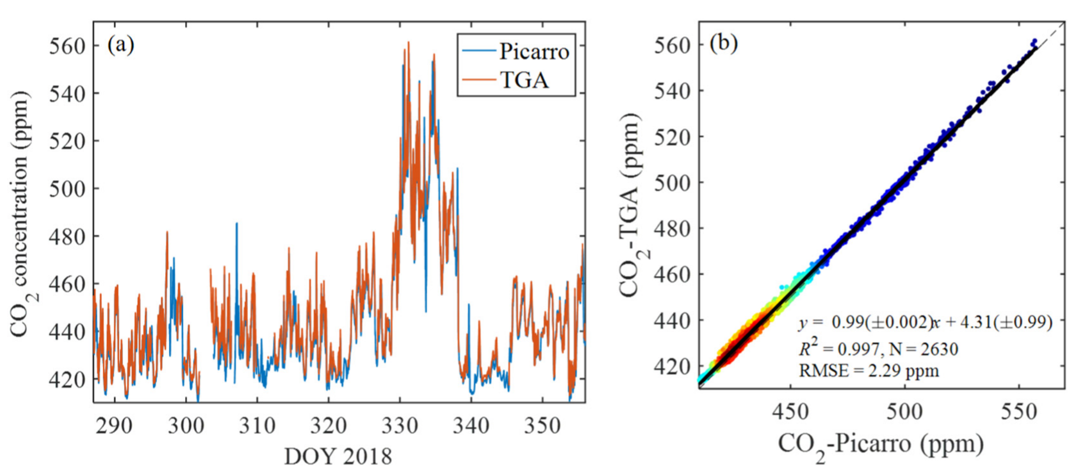

Fig. 6. Comparison of the CO_2 concentration measured with the Picarro analyzer and the closed-path EC TGA analyzer from 14 October to 21 December 2018: time series (a) and 1:1 plot (b). In panel b, color indicates data density. Also shown in panel b are regression statistics.

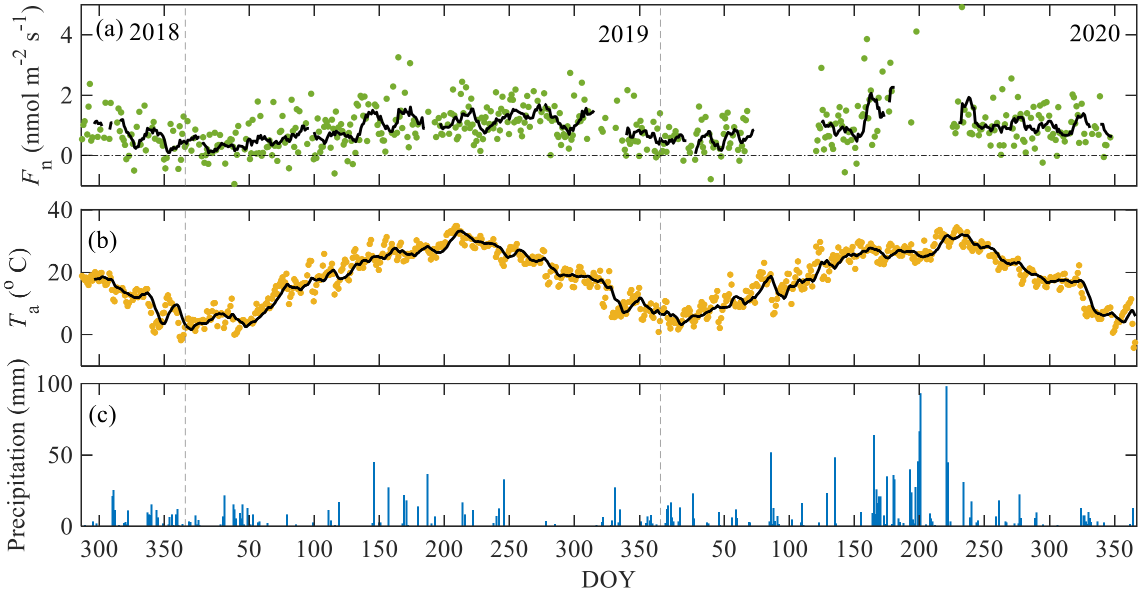

Fig. 7. Time series of (a) daily mean N_2O flux, (b) daily mean air temperature, and (c) daily precipitation over the whole measurement period. In panel a and b, filled dots represent daily mean values, and black lines represent 10-day running means.

1 standard deviation of spatial replicates) nmol m^{-2} s^{-1} for rice paddy and 0.58 ± 0.61 nmol m^{-2} s^{-1} for dryland crops. Our growing season value, 1.14 nmol m^{-2} s^{-1}, was significantly higher than both (one-sided Student *t*-test $p < 0.01$). For plot- and field-scale studies conducted over the annual period, the N_2O flux is 2.55 ± 2.44 kg N_2O-N ha^{-1} y^{-1} from rice-fallow systems, 6.65 ± 4.59 kg N_2O-N ha^{-1} y^{-1} for rice-dryland crop rotation, and 3.29 ± 7.44 kg N_2O-N ha^{-1} y^{-1} for dryland crops. The rice-dryland crop rotation systems have the highest annual mean flux presumably because of higher total N fertilizer use. Our annual mean flux, 8.11 kg N_2O-N ha^{-1} y^{-1}, was higher than the mean values of the three groups, and the difference was statistically significant between our flux and those of rice-fallow systems and dryland crops ($p < 0.01$).

4. Discussion

4.1. Negative N_2O flux

Over the whole experimental period, 66% of the daily flux value fell in the range from 0.2 to 1.4 nmol m^{-2} s^{-1} and 92% was positive (Fig. 12), indicating that the landscape was a source of N_2O most of the time. About 8% of the daily flux was negative, implying a net N_2O uptake. Negative N_2O flux has also been reported for cropland (maize, rice paddy and wheat; Li et al., 2008; Berger et al., 2013; Hao et al., 2016; Tallec et al., 2019), grassland (Jones et al., 2011), forests (Eugster et al., 2007; Zona et al., 2013b) and aquatic ecosystems (Huttunen et al., 2003; Xia et al., 2013). Low N and oxygen levels in the soil tend to favor N_2O consumption (Chapuis-Lardy et al., 2007). For rice paddies, negative N_2O flux has been reported for waterlogged periods (Berger et al., 2013; Hao et al., 2016). In our study, nearly all the negative flux was measured in the non-growing season, when most of the fields in the flux footprint were in the fallow/flooding phase of the rice-fallow rotation. The most negative flux (−0.96 nmol m^{-2} s^{-1}) was observed on 8 February 2019, one of the coldest days during the experiment (Fig. 7b; temperature on 8 February 2019 was −0.1 °C). Our results are consistent with the study of a subtropical rice paddy by Lin et al. (2012), who found that lower temperature and waterlogged condition are conducive to N_2O consumption by the soil.

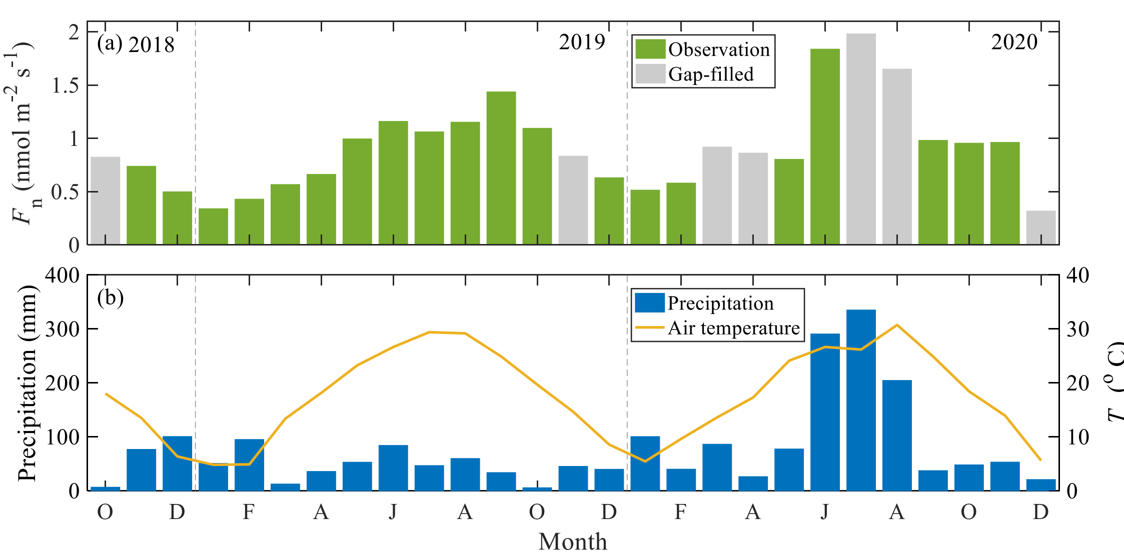

Fig. 8. Time series of (a) monthly mean N_2O flux, and (b) monthly mean air temperature and precipitation over the whole measurement period.

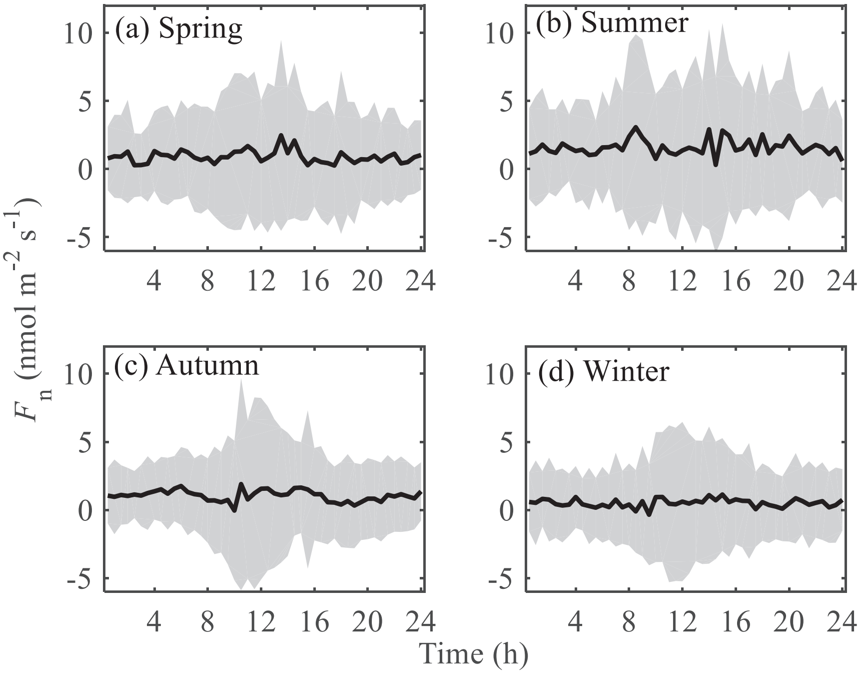

Fig. 9. Diurnal pattern of the N_2O flux for (a) spring, (b) summer, (c) autumn, and (d) winter during the whole measurement period. Solid lines are ensemble means and grey areas denote ± 1 standard deviation.

The negative flux cannot be explained by instrument calibration uncertainty (3%; Section 2.2). To obtain an estimate of the overall uncertainty of the daily flux, we selected a two-week period from 12 August to 25 August 2019 when weather conditions were relatively stable (no rain; mean daily temperature in the range of 27.6 to 31.5 °C), and assumed that the flux fluctuations were caused by measurement uncertainties. The standard deviation of the daily flux was 0.4 nmol m^{-2} s^{-1}. Because the zero flux value was more than two standard deviations away from the mean, the chance of a negative flux due to measurement uncertainty was less than 2%.

4.2. Temperature and precipitation controls on the N_2O flux

Previous plot- and field-scale studies often show periods of pulse-like N_2O flux resulting from fertilization use and precipitation or irrigation (Molodovskaya et al., 2012; Wang et al., 2013; Huang et al., 2014; Tallec et al., 2019). This phenomenon was not observed in this study (Fig. 7a) for two reasons. First, our flux footprint is extensive: the area encompassed by the 90% footprint contour line is about 200 km^2 (Fig. 1a). Timing of fertilizer application varied by several weeks among the fields in this footprint, so any fertilizer-induced emission signal associated with an individual farm would become smeared. Second, the footprint of any single half-hourly measurement was restricted to a small wind directional sector that may or may not have been affected by fertilizer application. The lack of flux pulses may also be an indication of a large contribution of indirect emission (from irrigation channels) to the observed flux.

The largest monthly flux was observed in June 2020, the month with the highest monthly precipitation (291 mm) of the whole experiment. The climatological mean precipitation for June is 165 mm. The month of June 2019 experienced the sixth lowest precipitation amount (84 mm) from 1990 to 2020, and the flux was 1.16 nmol m^{-2} s^{-1} or 59% lower than the value observed for June 2020. The air temperature in June was similar between the two years (26.6 °C in 2019 and 26.7 °C in 2020), further supporting the interpretation of the precipitation effect on the monthly flux. Heavier precipitation may have a larger influence on emissions from water bodies than from paddy fields, as more N is moved to the aquatic ecosystems by leaching and runoff, stimulating the production of N_2O (Tian et al., 2017). Further, previous studies of a rice-based agro-ecosystem in southeast China (Zheng et al., 2000) and a rice-dominated agricultural watershed in eastern China (Xiao et al., 2019a) show positive correlation between precipitation and the N_2O flux.

In the US Corn Belt, N_2O emission is enhanced by warmer and wetter conditions (Griffis et al., 2017). In the present study, temperature and precipitation also exerted positive influence on the monthly flux (Eq. (1)). On the annual time scale, precipitation variation may have contributed to the

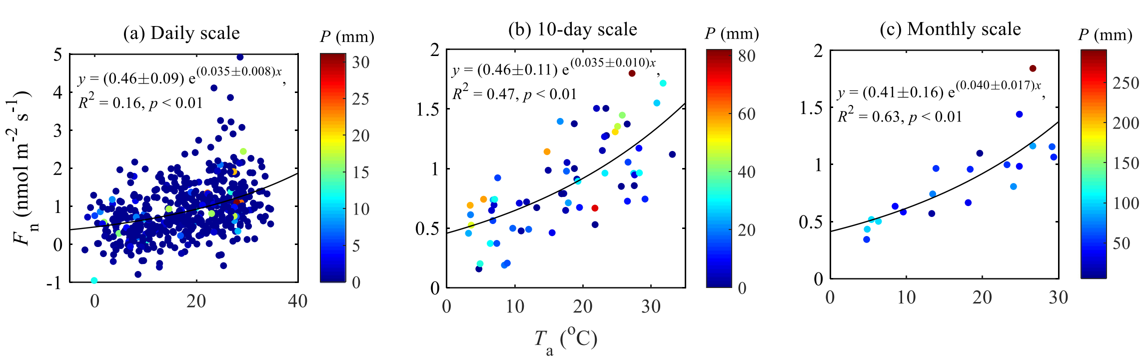

Fig. 10. Relationships of the N_2O flux with air temperature at the (a) daily, (b) 10-day and (c) monthly scale. Color in panels indicates precipitation amount (mm).

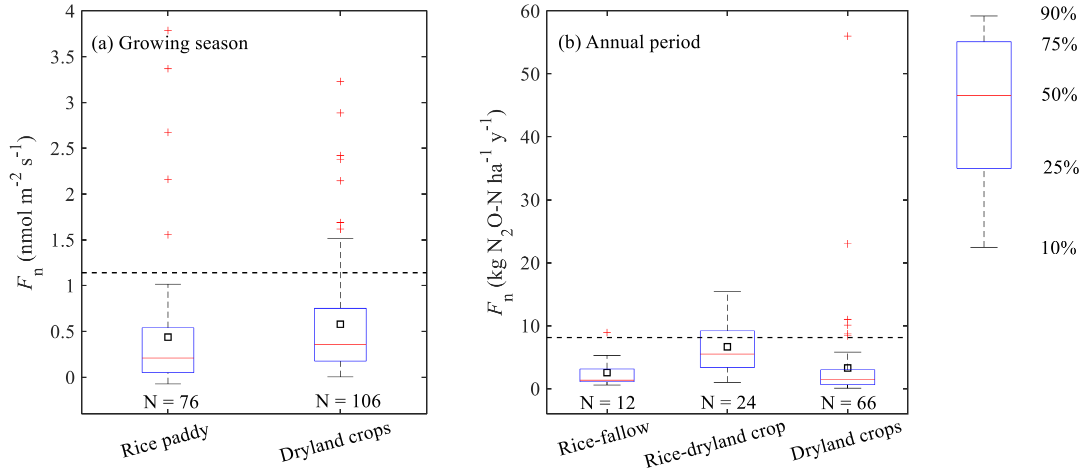

Fig. 11. Comparison with plot- and field-scale N_2O flux data found in the literature for the growing-season (a) and the annual period (b). Number of observations is denoted by N. Dashed lines represent the mean values of this study. Black square represents the mean value of each group. The + symbol represents outliers.

higher annual flux in 2020 (9.1 kg N_2O-N ha^{-1}, annual precipitation 1322 mm) than in 2019 (7.6 kg N_2O-N ha^{-1}, annual precipitation 564 mm) as the annual mean temperature was nearly the same between the two years (18.2 °C in 2019 and 18.0 °C in 2020). In Griffis et al. (2017), the interannual variability is much larger (85%) than ours (20%), and is driven primarily by temperature change. This comparison is preliminary because of different time span (six years versus two years) and different spatial scales (regional scale versus local scale).

A positive correlation between temperature and the N_2O flux has been reported for both terrestrial (e.g., Smith et al., 1998; Flessa et al., 2002; Hörtnagl and Wohlfahrt, 2014; Waldo et al., 2019) and aquatic ecosystems (e.g., Hu et al., 2012; Venkiteswaran et al., 2014; Wu et al., 2018; Xiao et al., 2019b; Grossel et al., 2021). The Q_{10} of the N_2O flux from terrestrial systems is in the range of 0.6 to 19.3 (Smith et al., 1998; Dobbie et al., 1999; Flessa et al., 2002; Zou et al., 2004; Parkin and Kaspar, 2006; Ding et al., 2007; Song and Zhang, 2009; Smith et al., 2011; Ni et al., 2012; Li et al., 2013; Zhou et al., 2018; Liu et al., 2019), with a mean value of 3.7,

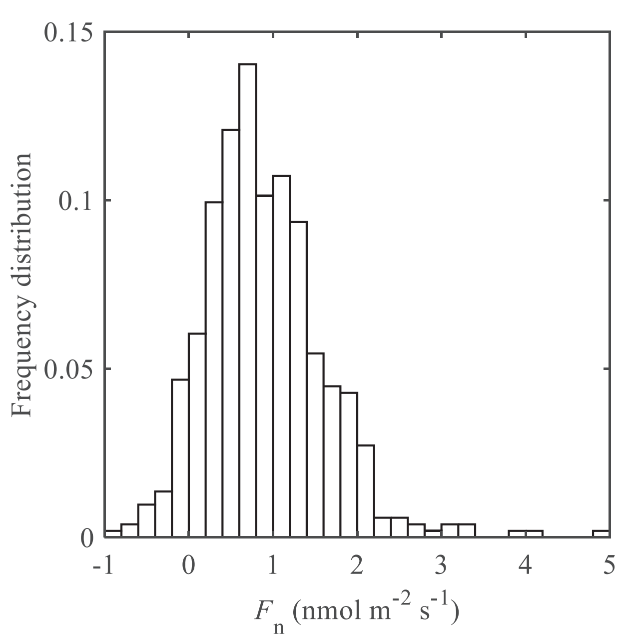

Fig. 12. Frequency distribution of the daily N_2O flux over the whole experimental period.

which is higher than the mean value of 2.7 for aquatic ecosystems (range 1.7 to 4.5, Liu et al., 2016; Xiao et al., 2019a; Xiao et al., 2019b). The Q_{10} in the present study, found by fitting the data in Fig. 10 with an exponential function across the three time scales, is between 1.4 and 1.5, which is near the lower limit of the above ranges. This result was 1 to 3 times lower than the value obtained for permanently flooded rice paddy fields in subtropical China (Q_{10} 3.3 to 6.1, Zhou et al., 2018). By performing an inverse analysis with the N_2O concentration observed on a tall tower, Griffis et al. (2017) found that the regional-scale Q_{10} for the US Corn Belt is also quite low (2.0). It appears that the N_2O flux has weaker response to temperature at the landscape and the regional scale than the plot- and field-scale flux, as the former may consist of sources with a weak temperature dependence.

4.3. Explanation for the high EC flux

Two reasons may explain the higher N_2O flux in our study than in other rice paddy studies. First, the N_2O flux data for rice paddies cited in Fig. 11 were all based on the chamber method. It is possible that some emission hotspots (locations of high emission) and hot moments (episodic high emission events) are missed by these small-scale measurements. Although some authors have reported good agreement in the N_2O flux between the chamber method and the EC method (Christensen et al., 1996; Hargreaves et al., 1996), others have found that the chamber method is biased low by as much as 50% on the annual time scale in comparison with the EC measurement (Wang et al., 2013; 1.43 kg N_2O-N ha^{-1} y^{-1} according to the chamber method and 3.15 kg N_2O-N ha^{-1} y^{-1} according to the EC method), suggesting that the EC may has measured a different area. Second, drainage systems are N_2O emission hotspots (Denmead et al., 2010; Turner et al., 2015), but they are generally omitted in the chamber-based studies. In the US Corn Belt, indirect N_2O emission from the drainage network and streams accounts for 53% of the total emission (Turner et al., 2015).

Currently, we lack direct evidence of large emission signals associated with drainage networks in the YRD. Xia et al. (2013) reported that the mean N_2O flux is 0.08 nmol m^{-2} s^{-1} for rivers, ponds and reservoirs in a small rice paddy watershed called Jurong (area of 45.5 km^2) in Jiangsu Province, China. In a later study of the same watershed but with expanded measurement to include small irrigation ditches, Xiao et al. (2019a) observed a higher mean N_2O flux of 0.31 nmol m^{-2} s^{-1}. These flux values are lower than those reported for irrigation ditches and rivers in the US Corn Belt (5.25 nmol m^{-2} s^{-1}; Turner et al., 2015) and lowland arable catchment in the UK (0.37 to 3.35 nmol m^{-2} s^{-1}; Outram and Hiscock, 2012), even though the reactive N concentrations in the Jurong watershed (NO_3-N = 0.30 to 1.85 mg L^{-1}, NH_4-N mg L^{-1} = 0.12 to 0.49 mg L^{-1}) are at similar levels as those reported by Outram and Hiscock (2012). In Xia et al. (2013) and Xiao et al. (2019a), the N_2O flux was measured two times per month using the water-air exchange method. Xiao et al. (2019a) suggest that because of the coarse temporal resolution, hot emission moments may have been missed. Continuous monitoring of riverine flux may be an important next step to determine whether the waterways in the flux footprint are the source of the high indirect emission flux suggested by our tall-tower data.

Another potential large emission source is aquaculture ponds. This is because they receive much more N input than cropland. According to our survey of local aquaculture farming practice, the annual N input was 1430 kg N ha^{-1}. Similarly high N inputs have been reported for aquaculture ponds in other areas (405 to 650 kg N ha^{-1}, Liu et al., 2016; Ma et al., 2018; Wu et al., 2018). Surprisingly, the N_2O flux reported for aquaculture ponds is relatively low, ranging from 0.02 to 0.36 nmol m^{-2} s^{-1} (Liu et al., 2016; Ma et al., 2018; Wu et al., 2018; Li et al., 2019; Yuan et al., 2019; Yang et al., 2020). To investigate the role of aquaculture ponds in the landscape N_2O budget, we measured the N_2O flux of two fishponds near the tall tower. Details about the fishpond measurement are described in Supplementary Materials. The pond flux was more sensitive to temperature (Q_{10} = 2.5, Supplementary Fig. S2) than the tall-tower flux (Q_{10}: 1.4 to 1.5, Fig. 9). The mean pond flux was 0.37 nmol m^{-2} s^{-1} over the period between January 2018 and October 2020 (Supplementary Fig. S1), which was 59% lower than the mean tall-tower flux. It should be noted that our pond measurement was made when the ponds were full of water, so were those reported by Wu et al. (2018), Yuan et al. (2019) and Yang et al. (2020). We hypothesize that the pond emission flux, driven by high sediment N concentrations, is much higher during low water levels and dry periods than when the pond is fully inundated (Liu et al., 2016; Ma et al., 2018). This hypothesis, if confirmed in future experiments in the tall-tower footprint, can partially reconcile the difference between our tall-tower flux and the plot- and field-scale observations (Fig. 11).

4.4. Emission factor

Combustion sources of N_2O in the EC footprint were negligible. The total number of residents was about 2000 to 4000 in the tower footprint. They used coal, liquid fuel and electricity for cooking. No space heating was allowed. Government regulations did not permit burning of crop residues in this region. With these considerations, the measured flux can be used to infer an emission factor.

Our footprint analysis revealed that 67% of the surface in the eddy flux footprint was occupied by cropland, 5% by aquaculture ponds, and the remaining by forest, water body, impervious area and other lands (Table S1). Among them, only cropland and aquaculture ponds were applied N fertilizer. Using the above footprint proportions and the N inputs, we arrived at a footprint-weighted fertilizer application intensity of 200 kg N ha^{-1} (Table S2). The annual N_2O emission from this agricultural landscape was 7.6 and 9.1 kg N_2O-N ha^{-1}, corresponding to 3.8% and 4.6% of the applied N in 2019 and 2020, respectively.

Our result was higher than the IPCC default direct emission factor (EF) of 1% (range 0.3% to 3%) for dryland crops and 0.3% (range 0.0% to 0.6%) for rice paddies (IPCC, 2006). The footprint-weighted direct EF using these two default values was 0.4% for the cropland in the eddy flux footprint. If we assume that this is the true direct EF, the indirect EF would be 3.4% to 4.2%, which is higher than the default EF (0.75%) of indirect emission resulting from N leaching and runoff (range 0.05% to 2.5%). Alternatively, if we accept the IPCC default indirect EF of 0.75%, our result would imply a direct EF of 3.05% to 3.85%, which is greater than the upper limit of the IPCC range for direct emission.

Our EF was lower than the US Corn Belt result (value 5.3% ± 1.2%) reported by Griffis et al. (2017). In that region, about 12% of the regional emission is contributed by livestock (Griffis et al., 2013). In our study, livestock emission was negligible as farm animal population (pigs and chickens) was small.

5. Conclusions

The present study appears to be the first effort to observe the N_2O flux with the EC method in a rice cultivation landscape. The landscape was a source of N_2O most of the time, with a daily mean flux of 0.90 ± 0.71 nmol m^{-2} s^{-1} over the 27-month measurement period. Air temperature and precipitation explained 78% of the monthly N_2O flux variations. The temperature sensitivity was rather low (Q_{10}: 1.4 to 1.5), supporting a previous study (Griffis et al., 2017) showing that the N_2O flux has weaker response to temperature at spatial scales consisting of multiple sources than at the plot scale consisting of a single soil source.

Our tall-tower flux was higher than most flux values found in other rice paddy studies. One explanation for this difference is that small-scale chamber measurements in those studies may have missed emission hot spots and hot moments. The large emission factors reported here imply that waterbodies in the flux footprint, such as aquaculture ponds with intensive N input and irrigation networks, are potentially large emission sources.

CRediT authorship contribution statement

Yanhong Xie: Conceptualization, Methodology, Formal analysis, Investigation, Writing-Original Draft, Writing-Review & Editing. **Mi Zhang**: Conceptualization, Methodology, Writing-Review & Editing, Supervision, Project administration, Funding acquisition. **Wei Xiao**: Conceptualization, Visualization, Supervision, Project administration, Funding acquisition. **Jiayu Zhao**: Conceptualization, Methodology, Formal analysis. **Wenjing Huang**: Software, Investigation. **Zhen Zhang**: Investigation, Data Curation. **Yongbo Hu**: Software, Investigation. **Zhihao Qin**: Formal analysis, Investigation. **Lei Jia**: Formal analysis, Investigation. **Yini Pu**: Formal analysis, Investigation. **Haoran Chu**: Formal analysis, Investigation. **Jiao Wang**: Investigation. **Jie Shi**: Investigation. **Shoudong Liu**: Resources, Supervision, Project administration. **Xuhui Lee**: Conceptualization, Methodology, Writing-Review & Editing.

Declaration of competing interest

The authors declare that they have no known competing financial interests or personal relationships that could have appeared to influence the work reported in this paper.

Acknowledgements

This research was supported by the National Key Research and Development Program of China (grant number 2020YFA0607501 to WX and MZ), the National Natural Science Foundation of China (grant numbers 41575147 to MZ, 41801093 and 41475141 to WX, 42021004 to WX and MZ), and open fund from the Key Laboratory of Meteorology and Ecological Environment of Hebei Province (Z201901H to WX).

Appendix A. Supplementary data

Supplementary data to this article can be found online at https://doi.org/10.1016/j.scitotenv.2021.152210.

References

Akiyama, H., Yagi, K., Yan, X.Y., 2005. Direct N2O emissions from rice paddy fields: summary of available data. Glob. Biogeochem. Cycles 19, GB1005.

Aubinet, M., Vesala, T., Papale, D., 2012. Eddy covariance: a practical guide to measurement and data analysis. Springer.

Barcza, Z., Kern, A., Haszpra, L., Kljun, N., 2009. Spatial representativeness of tall tower eddy covariance measurements using remote sensing and footprint analysis. Agric. For. Meteorol. 149, 795–807.

Barton, L., Butterbach-Bahl, K., Kiese, R., Murphy, D.V., 2011. Nitrous oxide fluxes from a grain–legume crop (narrow-leafed lupin) grown in a semiarid climate. Glob. Chang. Biol. 17, 1153–1166.

Berger, S., Jang, I., Seo, J., Kang, H., Gebauer, G., 2013. A record of N2O and CH4 emissions and underlying soil processes of Korean rice paddies as affected by different water management practices. Biogeochemistry 115, 317–332.

Brown, S.E., Sargent, S., Wagner-Riddle, C., 2018. Evaluation of a lower-powered analyzer and sampling system for eddy-covariance measurements of nitrous oxide fluxes. Atmos. Meas. Tech. 11, 1583–1597.

Butterbach-Bahl, K., Baggs, E.M., Dannenmann, M., Kiese, R., Zechmeister-Boltenstern, S., 2013. Nitrous oxide emissions from soils: how well do we understand the processes and their controls? Philos. Trans. R. Soc. B 368, 20130122.

Cabral, O.M., Freitas, H.C., Cuadra, S.V., de Andrade, C.A., Ramos, N.P., Grutzmacher, P., Galdosd, M., Packera, A.P.C., da Rochae, H.R., Rossi, P., 2020. The sustainability of a sugarcane plantation in Brazil assessed by the eddy covariance fluxes of greenhouse gases. Agric. For. Meteorol. 282, 107864.

Chapuis-Lardy, L., Wrage, N., Metay, A., Chotte, J., Bernoux, M., 2007. Soils, a sink for N2O? A review. Glob. Chang. Biol. 13, 1–17.

Christensen, S., Ambus, P., Arah, J.R.M., Clayton, H., Galle, B., Griffith, D.W.T., Hargreaves, K.J., Klemedtsson, L., Lind, A.M., Maag, M., Scott, A., Skiba, U., Smith, K.A., Welling, M., Wienhold, F.G., 1996. Nitrous oxide emission from an agricultural field: comparison between measurements by flux chamber and micrometerological techniques. Atmos. Environ. 30 (24), 4183–4190.

Cowan, N.J., Levy, P.E., Famulari, D., Anderson, M., Drewer, J., Carozzi, M., Reay, D.S., Skiba, U.M., 2016. The influence of tillage on N2O fluxes from an intensively managed grazed grassland in Scotland. Biogeosciences 13, 4811–4821.

Cowan, N., Levy, P., Maire, J., Coyle, M., Leeson, S.R., Famulari, D., Carozzic, M., Nemitza, E., Skiba, U., 2020. An evaluation of four years of nitrous oxide fluxes after application of ammonium nitrate and urea fertilisers measured using the eddy covariance method. Agric. For. Meteorol. 280, 107812.

Davis, K.J., Bakwin, P.S., Yi, C., Berger, B.W., Zhao, C., Teclaw, R.M., Isebrands, J.G., 2003. The annual cycles of CO2 and H2O exchange over a northern mixed forest as observed from a very tall tower. Glob. Chang. Biol. 9, 1278–1293.

Denmead, O.T., Macdonald, B.C.T., Bryant, G., Naylor, T., Wilson, S., Griffith, D.W., Wang, W.J., Salter, B., White, I., Moody, P.W., 2010. Emissions of methane and nitrous oxide from Australian sugarcane soils. Agric. For. Meteorol. 150, 748–756.

Desai, A.R., Xu, K., Tian, H.Q., Weishampel, P., Thom, J., Baumann, D., Andrewse, A.E., Cook, B.D., King, J.Y., Kolka, R., 2015. Landscape-level terrestrial methane flux observed from a very tall tower. Agric. For. Meteorol. 201, 61–75.

Di Marco, C., Skiba, U., Weston, K., Hargreaves, K., Fowler, D., 2004. Field scale N2O flux measurements from grassland using eddy covariance. Water Air Soil Pollut.: Focu 4, 143–149.

Ding, W.X., Cai, Y., Cai, Z.C., Yagi, K., Zheng, X.H., 2007. Nitrous oxide emissions from an intensively cultivated maize–wheat rotation soil in the North China plain. Sci. Total Environ. 373, 501–511.

Dobbie, K.E., McTaggart, I.P., Smith, K.A., 1999. Nitrous oxide emissions from intensive agricultural systems: variations between crops and seasons, key driving variables, and mean emission factors. J. Geophys. Res. Atmos. 104 (D21), 26891–26899.

Eugster, W., Zeyer, K., Zeeman, M., Michna, P., Zingg, A., Buchmann, N., Emmenegger, L., 2007. Methodical study of nitrous oxide eddy covariance measurements using quantum cascade laser spectrometery over a swiss forest. Biogeosciences 4, 927–939.

Famulari, D., Nemitz, E., Di Marco, C., Phillips, G.J., Thomas, R., House, E., Fowler, D., 2010. Eddy-covariance measurements of nitrous oxide fluxes above a city. Agric. For. Meteorol. 150, 786–793.

Flessa, H., Ruser, R., Schilling, R., Loftfield, N., Munch, J.C., Kaiser, E.A., Beese, F., 2002. N2O and CH4 fluxes in potato fields: automated measurement, management effects and temporal variation. Geoderma 105, 307–325.

Fuchs, K., Hörtnagl, L., Buchmann, N., Eugster, W., Snow, V., Merbold, L., 2018. Management matters: testing a mitigation strategy for nitrous oxide emissions using legumes on intensively managed grassland. Biogeosciences 15, 5519–5543.

Gong, P., Liu, H., Zhang, M.N., Li, C.C., Wang, J., Huang, H.B., Clinton, N., Ji, L.Y., Li, W.Y., Bai, Y.Q., Chen, B., Xu, B., Zhu, Z.L., Yuan, C., Suen, H.P., Guo, J., Nan Xu, N., Li, W.J., Zhao, Y.Y., Yang, J., Yu, C.Q., Wang, X., Fu, H.H., Yu, L., Dronova, I., Hui, F.M., Cheng, X., Shi, X.L., Xiao, F.J., Liu, Q.F., Song, L.C., 2019. Stable classification with limited sample: transferring a 30-m resolution sample set collected in 2015 to mapping 10-m resolution global land cover in 2017. Science Bulletin 64, 370–373.

Goodrich, J.P., Wall, A.M., Campbell, D.I., Fletcher, D., Wecking, A.R., Schipper, L.A., 2021. Improved gap filling approach and uncertainty estimation for eddy covariance N2O fluxes. Agric. For. Meteorol. 297, 108280.

Griffis, T.J., Lee, X.H., Baker, J.M., Russelle, M.P., Zhang, X., Venterea, R., Millet, D.B., 2013. Reconciling the differences between top-down and bottom-up estimates of nitrous oxide emissions for the US Corn Belt. Glob. Biogeochem. Cycles 27, 746–754.

Griffis, T.J., Chen, Z., Baker, J.M., Wood, J.D., Millet, D.B., Lee, X.H., Ventereaa, R.T., Turner, P.A., 2017. Nitrous oxide emissions are enhanced in a warmer and wetter world. Proc. Natl. Acad. Sci. 114 (45), 12081–12085.

Grossel, A., Bourennane, H., Ayzac, A., Pasquier, C., Hénault, C., 2021. Indirect emissions of nitrous oxide in a cropland watershed with contrasting hydrology in Central France. Sci. Total Environ. 766, 142664.

Hao, Q.J., Jiang, C.S., Chai, X.S., Huang, Z., Fan, Z.W., Xie, D.T., He, X.H., 2016. Drainage, no-tillage and crop rotation decreases annual cumulative emissions of methane and nitrous oxide from a rice field in Southwest China. Agric. Ecosyst. Environ. 233, 270–281.

Hargreaves, K.J., Wienhold, F.G., Klemedtsson, L., Arah, J.R.M., Beverland, I.J., Fowler, D., Galle, B., Griffith, D.W.T., Skiba, U., Smith, K.A., Welling, M., Harris, G.W., 1996. Measurement of nitrous oxide emission from agricultural land using micrometeorological methods. Atmos. Environ. 30, 1563–1571.

Haszpra, L., Barcza, Z., Davis, K.J., Tarczay, K., 2005. Long-term tall tower carbon dioxide flux monitoring over an area of mixed vegetation. Agric. For. Meteorol. 132, 58–77.

Haszpra, L., Hidy, D., Taligás, T., Barcza, Z., 2018. First results of tall tower based nitrous oxide flux monitoring over an agricultural region in Central Europe. Atmos. Environ. 176, 240–251.

Helfter, C., Tremper, A.H., Halios, C.H., Kotthaus, S., Bjorkegren, A., Grimmond, C.S.B., Barlow, J.F., Nemitz, E., 2016. Spatial and temporal variability of urban fluxes of methane, carbon monoxide and carbon dioxide above LondonUK. Atmos. Chem. Phys. 16, 10543–10557.

Hörtnagl, L., Wohlfahrt, G., 2014. Methane and nitrous oxide exchange over a managed hay meadow. Biogeosciences 11, 7219–7236.

Hsieh, C.I., Leahy, P., Kiely, G., Li, C.S., 2005. The effect of future climate perturbations on N2O emissions from a fertilized humid grassland. Nutr. Cycl. Agroecosyst. 73, 15–23.

Hu, Z., Lee, J.W., Chandran, K., Kim, S., Khanal, S.K., 2012. Nitrous oxide (N2O) emission from aquaculture: a review. Environ. Sci. Technol. 46, 6470–6480.

Huang, H., Wang, J., Hui, D., Miller, D.R., Bhattarai, S., Dennis, S., Smart, D., Sammis, T., Reddy, K.C., 2014. Nitrous oxide emissions from a commercial cornfield (Zea mays) measured using the eddy covariance technique. Atmos. Chem. Phys. 14, 12839–12854.

Huang, W.J., Griffis, T.J., Hu, C., Xiao, W., Lee, X.H., 2021. Seasonal variations of CH4 emissions in the Yangtze River Delta region of China are driven by agricultural activities. Adv. Atmos. Sci. 38 (9), 1537–1551.

Huttunen, J.T., Alm, J., Liikanen, A., Juutinen, S., Larmola, T., Hammar, T., Silvola, J., Martikainen, P.J., 2003. Fluxes of methane, carbon dioxide and nitrous oxide in boreal lakes and potential anthropogenic effects on the aquatic greenhouse gas emissions. Chemosphere 52, 609–621.

IPCC, 2006. 2006 IPCC guidelines for national greenhouse gas inventories, prepared by the National Greenhouse gas Inventories Programme. Retrieved from Japan: www.ipcc-nggip.iges.or.jp/public/2006gl/.

Järvi, L., Nordbo, A., Rannik, Ü., Haapanala, S., Riikonen, A., Mammarella, I., Pihlatie, M., Vesala, T., 2014. Urban nitrous-oxide fluxes measured using the eddy-covariance technique in Helsinki, Finland. Boreal Env. Res. 19 (Suppl. B), 108–121.

Jones, S.K., Famulari, D., Di Marco, C.F., Nemitz, E., Skiba, U.M., Rees, R.M., Sutton, M.A., 2011. Nitrous oxide emissions from managed grassland: a comparison of eddy covariance and static chamber measurements. Atmos. Meas. Tech. 4, 2179–2194.

Kaimal, J.C., Wyngaard, J.C.J., Izumi, Y., Coté, O.R., 1972. Spectral characteristics of surface-layer turbulence. Quart. J. R. Met. Soc. 98, 563–589.

Kim, D.G., Mishurov, M., Kiely, G., 2010. Effect of increased N use and dry periods on N2O emission from a fertilized grassland. Nutr. Cycl. Agroecosyst. 88, 397–410.

Kljun, N., Calanca, P., Rotach, M.W., Schmid, H.P., 2015. A simple two-dimensional parameterisation for flux footprint prediction (FFP). Geosci. Model Dev. 8, 3695–3713.

Kroon, P.S., Hensen, A., Jonker, H.J.J., Zahniser, M.S., Van't Veen, W.H., Vermeulen, A.T., 2007. Suitability of quantum cascade laser spectroscopy for CH4 and N2O eddy covariance flux measurements. Biogeosciences 4, 715–728.

Kroon, P.S., Hensen, A., Jonker, H.J.J., Ouwersloot, H.G., Vermeulen, A.T., Bosveld, F.C., 2010a. Uncertainties in eddy covariance flux measurements assessed from CH4 and N2O observations. Agric. For. Meteorol. 150 (6), 806–816.

Kroon, P.S., Schrier-Uijl, A.P., Hensen, A., Veenendaal, E.M., Jonker, H.J.J., 2010b. Annual balances of CH4 and N2O from a managed fen meadow using eddy covariance flux measurements. Eur.J. Soil Sci. 61, 773–784.

Leahy, P., Kiely, G., Scanlon, T.M., 2004. Managed grasslands: a greenhouse gas sink or source? Geophys. Res. Lett. 31, L20507.

Lee, X.H., 2018. Fundamentals of Boundary-Layer Meteorology. Springer, Berlin.

Li, J., Tong, X.J., Yu, Q., Dong, Y.S., Peng, C.H., 2008. Micrometeorological measurements of nitrous oxide exchange above a cropland. Atmos. Environ. 42, 6992–7001.

Li, L.J., Han, X.Z., You, M.Y., Horwath, W.R., 2013. Nitrous oxide emissions from mollisols as affected by long-term applications of organic amendments and chemical fertilizers. Sci. Total Environ. 452, 302–308.

Li, F.B., Feng, J.F., Zhou, X.Y., Xu, C.C., Jijakli, M.H., Zhang, W.J., Fang, F.P., 2019. Impact of rice-fish/shrimp co-culture on the N2O emission and NH3 volatilization in intensive aquaculture ponds. Sci. Total Environ. 655, 284–291.

Liang, L.L., Campbell, D.I., Wall, A.M., Schipper, L.A., 2018. Nitrous oxide fluxes determined by continuous eddy covariance measurements from intensively grazed pastures: temporal patterns and environmental controls. Agric. Ecosyst. Environ. 268, 171–180.

Lin, S., Iqbal, J., Hu, R., Ruan, L.L., Wu, J.S., Zhao, J.S., Wang, P.J., 2012. Differences in nitrous oxide fluxes from red soil under different land uses in mid-subtropical China. Agric. Ecosyst. Environ. 146, 168–178.

Linquist, B., Van Groenigen, K.J., Adviento-Borbe, M.A., Pittelkow, C., Van Kessel, C., 2012. An agronomic assessment of greenhouse gas emissions from major cereal crops. Glob. Chang. Biol. 18, 194–209.

Liu, S.W., Hu, Z.Q., Wu, S.Q., Li, S., Li, Z.F., Zou, J.W., 2016. Methane and nitrous oxide emissions reduced following conversion of rice paddies to inland crab–fish aquaculture in Southeast China. Environ. Sci. Technol. 50, 633–642.

Liu, C.Y., Hu, X.X., Zhang, W., Zheng, X.H., Wang, R., Yao, Z.S., Cao, G.M., 2019. Year-round measurements of nitrous oxide emissions and direct emission factors in extensively managed croplands under an alpine climate. Agric. For. Meteorol. 274, 18–28.

Lognoul, M., Debacq, A., De Ligne, A., Dumont, B., Manise, T., Bodson, B., Heinescha, B., Aubinet, M., 2019. N2O flux short-term response to temperature and topsoil disturbance in a fertilized crop: an eddy covariance campaign. Agric. For. Meteorol. 271, 193–206.

Ma, Y.C., Sun, L.Y., Liu, C.Y., Yang, X.Y., Zhou, W., Yang, B., Schwenke, G., Liu, D.L., 2018. A comparison of methane and nitrous oxide emissions from inland mixed-fish and crab aquaculture ponds. Sci. Total Environ. 637, 517–523.

Mammarella, I., Werle, P., Pihlatie, M., Eugster, W., Haapanala, S., Kiese, R., Markkanen, T., Rannik, U., Vesala, T., 2010. A case study of eddy covariance flux of N2O measured within forest ecosystems: quality control and flux error analysis. Biogeosciences 7, 427–440.

Mauder, M., Foken, T., 2004. Documentation and Instruction Manual of the Eddy Covariance Software Package TK2. University of Bayreuth, Department of Micrometeorology, Arbeitsergebnisse Nr. 26 42 pp.

Merbold, L., Eugster, W., Stieger, J., Zahniser, M., Nelson, D., Buchmann, N., 2014. Greenhouse gas budget (CO2, CH4 and N2O) of intensively managed grassland following restoration. Glob. Chang. Biol. 20, 1913–1928.

Mishurov, M., Kiely, G., 2010. Nitrous oxide flux dynamics of grassland undergoing afforestation. Agric. Ecosyst. Environ. 139, 59–65.

Mishurov, M., Kiely, G., 2011. Gap-filling techniques for the annual sums of nitrous oxide fluxes. Agric. For. Meteorol. 151, 1763–1767.

Molodovskaya, M., Warland, J., Richards, B.K., Öberg, G., Steenhuis, T.S., 2011. Nitrous oxide from heterogeneous agricultural landscapes: source contribution analysis by eddy covariance and chambers. Soil Sci. Soc. Am. J. 75, 1829–1838.

Molodovskaya, M., Singurindy, O., Richards, B.K., Warland, J., Johnson, M.S., Steenhuis, T.S., 2012. Temporal variability of nitrous oxide from fertilized croplands: hot moment analysis. Soil Sci. Soc. Am. J. 76, 1728–1740.

Moncrieff, J.B., Massheder, J.M., De Bruin, H., Elbers, J., Friborg, T., Heusinkveld, B., Kabat, P., Scott, S., Soegaard, H., Verhoef, A., 1997. A system to measure surface fluxes of momentum, sensible heat, water vapour and carbon dioxide. J. Hydrol. 188, 589–611.

Neftel, A., Flechard, C., Ammann, C., Conen, F., Emmenegger, L., Zeyer, K., 2007. Experimental assessment of N2O background fluxes in grassland systems. Tellus Ser. B Chem. Phys. Meteorol. 59, 470–482.

Neftel, A., Ammann, C., Fischer, C., Spirig, C., Conen, F., Emmenegger, L., Tuzson, B., Wahlen, S., 2010. N2O exchange over managed grassland: application of a quantum cascade laser spectrometer for micrometeorological flux measurements. Agric. For. Meteorol. 150, 775–785.

Nemitz, E., Mammarella, I., Ibrom, A., Aurela, M., Burba, G.G., Dengel, S., Gielen, B., Grelle, A., Heinesch, B., Herbst, M., Hörtnagl, L., Klemedtsson, L., Lindroth, A., Lohila, A., McDermitt, D.K., Meier, P., Merbold, L., Nelson, D., Nicolini, G., Nilsson, M.B., Peltola, O., Rinne, J., Zahniser, M., 2018. Standardisation of eddy-covariance flux measurements of methane and nitrous oxide. Int. Agrophys. 32, 517–549.

Ni, K., Ding, W.X., Zaman, M., Cai, Z.C., Wang, Y.F., Zhang, X.L., Zhou, B.K., 2012. Nitrous oxide emissions from a rainfed-cultivated black soil in Northeast China: effect of fertilization and maize crop. Biol. Fertil. Soils 48, 973–979.

Nicolini, G., Castaldi, S., Fratini, G., Valentini, R., 2013. A literature overview of micrometeorological CH4 and N2O flux measurements in terrestrial ecosystems. Atmos. Environ. 81, 311–319.

Outram, F.N., Hiscock, K.M., 2012. Indirect nitrous oxide emissions from surface water bodies in a lowland arable catchment: a significant contribution to agricultural greenhouse gas budgets? Environ. Sci. Technol. 46, 8156–8163.

Parkin, T.B., Kaspar, T.C., 2006. Nitrous oxide emissions from corn–soybean systems in the Midwest. J. Environ. Qual. 35, 1496–1506.

Pattey, E., Blackburn, L.G., Strachan, I.B., Desjardins, R., Dow, D., 2008. Spring thaw and growing season N2O emissions from a field planted with edible peas and a cover crop. Can. J. Soil Sci. 88, 241–249.

Peltola, O., Hensen, A., Marchesini, L.B., Helfter, C., Bosveld, F.C., van den Bulk, W.C.M., Haapanala, S., van Huissteden, J., Laurila, T., Lindroth, A., Nemitz, E., Röckmann, T., Vermeulen, A.T., Mammarella, I., 2015. Studying the spatial variability of methane flux with five eddy covariance towers of varying height. Agric. For. Meteorol. 214, 456–472.

Pihlatie, M., Rinne, J., Ambus, P., Pilegaard, K., Dorsey, J.R., Rannik, Ü., Markkanen, T., Launiainen, S., Vesala, T., 2005. Nitrous oxide emissions from a beech forest floor measured by eddy covariance and soil enclosure techniques. Biogeosciences 2, 377–387.

Pihlatie, M.K., Kiese, R., Brueggemann, N., Butterbach-Bahl, K., Kieloaho, A.J., Laurila, T., Mammarella, I., Minkkinen, K., Penttila, T., Schonborn, J., Vesala, T., 2010. Greenhouse gas fluxes in a drained peatland forest during spring frost-thaw event. Biogeosciences 7, 1715–1727.

Qin, Y.M., Liu, S.W., Guo, Y.Q., Liu, Q.H., Zou, J.W., 2010. Methane and nitrous oxide emissions from organic and conventional rice cropping systems in Southeast China. Biol. Fertil. Soils 46, 825–834.

Rannik, Ü., Haapanala, S., Shurpali, N.J., Mammarella, I., Lind, S., Hyvönen, N., Peltola, O., Zahniser, M., Vesala, T., 2015. Intercomparison of fast response commercial gas analysers for nitrous oxide flux measurements under field conditions. Biogeosciences 12, 415–432.

Scanlon, T.M., Kiely, G., 2003. Ecosystem-scale measurements of nitrous oxide fluxes for an intensely grazed, fertilized grassland. Geophys. Res. Lett. 30 (16), 1852.

Shcherbak, I., Millar, N., Robertson, G.P., 2014. Global metaanalysis of the nonlinear response of soil nitrous oxide (N2O) emissions to fertilizer nitrogen. Proc. Natl. Acad. Sci. 111 (25), 9199–9204.

Shurpali, N.J., Rannik, Ü., Jokinen, S., Lind, S., Biasi, C., Mammarella, I., Peltola, O., Pihlatie, M., Hyvönen, N., Räty, M., Haapanala, S., Zahniser, M., Virkajärvi, P., Vesala, T., Martikainen, P.J., 2016. Neglecting diurnal variations leads to uncertainties in terrestrial nitrous oxide emissions. Sci. Rep. 6, 25739.

Skiba, U., Hargreaves, K.J., Beverland, I.J., O'Neill, D.H., Fowler, D., Moncrieff, J.B., 1996. Measurement of field scale N2O emission fluxes from a wheat crop using micrometeorological techniques. Plant and Soil 181, 139–144.

Smith, K.A., Dobbie, K.E., 2001. The impact of sampling frequency and sampling times on chamber-based measurements of N2O emissions from fertilized soils. Glob. Chang. Biol. 57, 933–945.

Smith, K.A., Thomson, P.E., Clayton, H., McTaggart, I.P., Conen, F., 1998. Effects of temperature, water content and nitrogen fertilisation on emissions of nitrous oxide by soils. Atmos. Environ. 32 (19), 3301–3309.

Smith, D.R., Hernandez-Ramirez, G., Armstrong, S.D., Bucholtz, D.L., Stott, D.E., 2011. Fertilizer and tillage management impacts on non-carbon-dioxide greenhouse gas emissions. Soil Sci. Soc. Am. J. 75, 1070–1082.

Song, C.C., Zhang, J.B., 2009. Effects of soil moisture, temperature, and nitrogen fertilization on soil respiration and nitrous oxide emission during maize growth period in Northeast China. Acta Agric. Scand. Sec.t B: Soil Plant Sc. 59, 97–106.

Tallec, T., Brut, A., Joly, L., Dumelié, N., Serça, D., Mordelet, P., Claveriea, N., Legaind, D., Barriéd, J., Decarpenterieb, T., Cousinb, J., Zawilskia, B., Ceschiaa, E., Guérine, F., Le Dantec, V., 2019. N2O flux measurements over an irrigated maize crop: a comparison of three methods. Agric. For. Meteorol. 264, 56–72.

Tian, L.L., Zhu, B., Akiyama, H., 2017. Seasonal variations in indirect N2O emissions from an agricultural headwater ditch. Biol. Fertil. Soils 53, 651–662.

Tian, H.Q., Xu, R.T., Canadell, J.G., Thompson, R.L., Winiwarter, W., Suntharalingam, P., Davidson, E.A., Ciais, P., Jackson, R.B., Janssens-Maenhout, G., Prather, M.J., Regnier, P., Pan, N.Q., Pan, S.F., Peters, G.P., Shi, H., Tubiello, F.N., Zaehle, S., Zhou, F., Arneth, A., Battaglia, G., Berthet, S., Bopp, L., Bouwman, A.F., Buitenhuis, E.T., Chang, J.F., Chipperfield, M.P., Dangal, S.R.S., Dlugokencky, E., Elkins, J.W., Eyre, B.D., Fu, B.J., Hall, B., Ito, A., Joos, F., Krummel, P.B., Landolfi, A., Laruelle, G.G., Lauerwald, R., Li, W., Lienert, S., Maavara, T., MacLeod, M., Millet, D.B., Olin, S., Patra, P.K., Prinn, R.G., Raymond, P.A., Ruiz, D.J., van der Werf, G.R., Vuichard, N., Wang, J.J., Weiss, R.F., Wells, K.C., Wilson, C., Yang, J., Yao, Y.Z., 2020. A comprehensive quantification of global nitrous oxide sources and sinks. Nature 586, 248–256.

Turner, P.A., Griffis, T.J., Lee, X.H., Baker, J.M., Venterea, R.T., Wood, J.D., 2015. Indirect nitrous oxide emissions from streams within the US Corn Belt scale with stream order. Proc. Natl. Acad. Sci. 112 (32), 9839–9843.

Venkiteswaran, J.J., Rosamond, M.S., Schiff, S.L., 2014. Nonlinear response of riverine N2O fluxes to oxygen and temperature. Environ. Sci. Technol. 48, 1566–1573.

Vickers, D., Mahrt, L., 1997. Quality control and flux sampling problems for tower and aircraft data. J. Atmos. Ocean. Technol. 14, 512–526.

Voglmeier, K., Six, J., Jocher, M., Ammann, C., 2020. Soil greenhouse gas budget of two intensively managed grazing systems. Agric. For. Meteorol. 287, 107960.

Wagner-Riddle, C., Furon, A., Mclaughlin, N.L., Lee, I., Barbeau, J., Jayasundara, S., Parkin, G., von Bertoldi, P., Warland, J., 2007. Intensive measurement of nitrous oxide emissions from a corn-soybean-wheat rotation under two contrasting management systems over 5 years. Glob. Chang. Biol. 13, 1722–1736.

Waldo, S., Russell, E.S., Kostyanovsky, K., Pressley, S.N., O'Keeffe, P.T., Huggins, D.R., Stöckle, C.O., Pan, W.L., Lamb, B.K., 2019. N2O emissions from two agroecosystems: high spatial variability and long pulses observed using static chambers and the flux-gradient technique. J. Geophys. Res. Biogeosci. 124, 1887–1904.

Wang, K., Zheng, X.H., Pihlatie, M., Vesala, T., Liu, C.Y., Haapanala, S., Mammarella, I., Rannik, Ü., Liu, H.Z., 2013. Comparison between static chamber and tunable diode laser-based eddy covariance techniques for measuring nitrous oxide fluxes from a cotton field. Agric. For. Meteorol. 171, 9–19.

Wang, D., Wang, K., Zheng, X.H., Butterbach-Bahl, K., Díaz-Pinés, E., Chen, H., 2020. Applicability of a gas analyzer with dual quantum cascade lasers for simultaneous measurements of N2O, CH4 and CO2 fluxes from cropland using the eddy covariance technique. Sci. Total Environ. 729, 138784.

Webb, E.K., Pearman, G.I., Leuning, R., 1980. Correction of flux measurements for density effects due to heat and water vapour transfer. Q. J. R. Meteorol. Soc. 106, 85–100.

Wolf, B., Merbold, L., Decock, C., Tuzson, B., Harris, E., Six, J., Emmenegger, L., Mohn, J., 2015. First on-line isotopic characterization of N2O above intensively managed grassland. Biogeosciences 12, 2517–2531.

Wu, S., Hu, Z.Q., Hu, T., Chen, J., Yu, K., Zou, J.W., Liu, S.W., 2018. Annual methane and nitrous oxide emissions from rice paddies and inland fish aquaculture wetlands in Southeast China. Atmos. Environ. 175, 135–144.

Xia, Y.Q., Li, Y.F., Ti, C.P., Li, X.B., Zhao, Y.Q., Yan, X.Y., 2013. Is indirect N2O emission a significant contributor to the agricultural greenhouse gas budget? A case study of a rice paddy-dominated agricultural watershed in eastern China. Atmos. Environ. 77, 943–950.

Xiao, Q.T., Hu, Z.H., Fu, C.S., Bian, H., Lee, X.H., Chen, S.T., Shang, D.Y., 2019a. Surface nitrous oxide concentrations and fluxes from water bodies of the agricultural watershed in eastern China. Environ. Pollut. 251, 185–192.

Xiao, Q.T., Xu, X.F., Zhang, M., Duan, H.T., Hu, Z.H., Wang, W., Xiao, W., Lee, X.H., 2019b. Coregulation of nitrous oxide emissions by nitrogen and temperature in China's third largest freshwater Lake (Lake Taihu). Limnol. Oceanogr. 64, 1070–1086.

Yang, P., Yang, H., Lai, D.Y., Guo, Q.Q., Zhang, Y.F., Tong, C., Xu, C.B., Li, X.F., 2020. Large contribution of non-aquaculture period fluxes to the annual N2O emissions from aquaculture ponds in Southeast China. J. Hydrol. 582, 124550.

Yao, Z., Du, Y., Tao, Y., Zheng, X., Liu, C., Lin, S., Butterbach-Bahl, K., 2014. Water-saving ground cover rice production system reduces net greenhouse gas fluxes in an annual rice-based cropping system. Biogeosciences 11 (22), 6221–6236.

Yuan, J.J., Xiang, J., Liu, D.Y., Kang, H., He, T.H., Kim, S., Lin, Y.X., Freeman, C., Ding, W.X., 2019. Rapid growth in greenhouse gas emissions from the adoption of industrial-scale aquaculture. Nat. Clim. Chang. 9, 318–322.

Zenone, T., Zona, D., Gelfand, I., Gielen, B., Camino-Serrano, M., Ceulemans, R., 2016. CO2 uptake is offset by CH4 and N2O emissions in a poplar short-rotation coppice. GCB Bioenergy 8, 524–538.

Zhang, X., Davidson, E.A., Mauzerall, D.L., Searchinger, T.D., Dumas, P., Shen, Y., 2015. Managing nitrogen for sustainable development. Nature 528, 51–59.

Zheng, X.H., Wang, M.X., Wang, Y.S., Shen, R.X., Gou, J., Li, J., Jin, J.S., Li, L.T., 2000. Impacts of soil moisture on nitrous oxide emission from croplands: a case study on the rice-based agro-ecosystem in Southeast China. Chemos. Glob. Chang. Sci. 2, 207–224.

Zheng, X.H., Han, S.H., Huang, Y., Wang, Y.S., Wang, M.X., 2004. Re-quantifying the emission factors based on field measurements and estimating the direct N2O emission from chinese croplands. Glob. Biogeochem. Cycles 18, GB2018.

Zhou, M.H., Wang, X.G., Wang, Y.Q., Zhu, B., 2018. A three-year experiment of annual methane and nitrous oxide emissions from the subtropical permanently flooded rice paddy

fields of China: emission factor, temperature sensitivity and fertilizer nitrogen effect. Agric. For. Meteorol. 250, 299–307.
Zona, D., Janssens, I.A., Aubinet, M., Gioli, B., Vicca, S., Fichot, R., Ceulemans, R., 2013a. Fluxes of the greenhouse gases (CO2, CH4 and N2O) above a short-rotation poplar plantation after conversion from agricultural land. Agric. For. Meteorol. 169, 100–110.
Zona, D., Janssens, I.A., Gioli, B., Jungkunst, H.F., Serrano, M.C., Ceulemans, R., 2013b. N2O fluxes of a bio-energy poplar plantation during a two years rotation period. GCB Bioenergy 5, 536–547.
Zou, J.W., Huang, Y., Zong, L.G., Zheng, X.H., Wang, Y.S., 2004. Carbon dioxide, methane, and nitrous oxide emissions from a rice-wheat rotation as affected by crop residue incorporation and temperature. Adv. Atmos. Sci. 21 (5), 691–698.
Zou, J.W., Huang, Y., Lu, Y.Y., Zheng, X.H., Wang, Y.S., 2005. Direct emission factor for N2O from rice–winter wheat rotation systems in Southeast China. Atmos. Environ. 39, 4755–4765.